Article

Roles and Influences of Kerosene on Chalcopyrite Flotation in MgCl₂ Solution: EDLVO and DFT Approaches

Wanqing Li [1,2], **Yubiao Li** [1,2,3,]*, **Shaobing Xie** [1,2], **Wanqing Duan** [1,2] **and Wen Chen** [4,]*

1   Hubei Key Laboratory of Mineral Resources Processing and Environment, Wuhan University of Technology, Wuhan 430070, China; Wanqing.Li@whut.edu.cn (W.L.); Shaobing.Xie@whut.edu.cn (S.X.); wanqing.duan@whut.edu.cn (W.D.)
2   School of Resources and Environmental Engineering, Wuhan University of Technology, Wuhan 430070, China
3   State Key Laboratory of Complex Nonferrous Metal Resources Clean Utilization, Kunming 650093, China
4   Changsha Research Institute of Mining and Metallurgy Co., Ltd., Changsha 410012, China
*   Correspondence: Yubiao.Li@whut.edu.cn (Y.L.); wenchen@minmetals.com (W.C.)

Abstract: Seawater has been increasingly used as an alternative to freshwater in mineral flotation. Although previous studies suggest that Mg^{2+} ions in seawater have the primary negative roles in chalcopyrite flotation, insufficient work has been conducted to understand the effects of kerosene as a collector in chalcopyrite flotation. In this study, the influence of kerosene emulsion on chalcopyrite floatability in a solution containing Mg^{2+} was systematically investigated. The results indicated that the addition of kerosene significantly reduced the adsorption of hydrophilic Mg-precipitates onto the chalcopyrite's surface. In addition to contact angle, zeta potential, optical microscopy, and Fourier-transform infrared spectroscopy analyses, extended Derjguin–Landau–Verwey–Overbeek (EDLVO) theory and density functional theory (DFT) calculations were conducted to understand the influencing mechanisms of kerosene on chalcopyrite flotation. The adsorption energies showed an order of kerosene and $Mg(OH)_2$ > kerosene and chalcopyrite > chalcopyrite and $Mg(OH)_2$, indicating kerosene was preferentially adsorbed on the $Mg(OH)_2$ surface, forming agglomerates and therefore reducing the adsorption of $Mg(OH)_2$ precipitates onto the chalcopyrite's surface. In addition, hydrophobic agglomerates were also formed due to the attachment of kerosene to the chalcopyrite's surface when additional kerosene was added, further enhancing chalcopyrite floatability.

Keywords: chalcopyrite; seawater; flotation; kerosene emulsion; mechanism

1. Introduction

Copper, a very important nonferrous metal closely related to human life, is widely used in many fields, including the electric, electronic, and automotive industries. Specifically, nearly 70% of Earth's cupriferous resource is obtained from chalcopyrite [1,2]. In industry, chalcopyrite is usually concentrated by a flotation process, which is a water-intensive process consuming vast amounts of freshwater. However, freshwater is limited due to the increasing scarcity of freshwater resources and stringent environmental regulations [3,4]. The main water resource, seawater, which accounts for 97% of the Earth's water resource, is therefore considered as an alternative for flotation, thereby minimizing freshwater usage, especially for those located in freshwater-deficient areas, such as Australia and Chile [4,5].

However, previous studies showed that the inevitable ions present in seawater (e.g., Mg^{2+}, Ca^{2+}, K^+, Na^+, Cl^-, and $SO_4{}^{2-}$) not only affect water structure, but also change the properties of the mineral surface and mineral–bubble interaction during flotation [4,6–8]. Specifically, the presence of Mg^{2+} in seawater significantly depressed mineral flotation [1,9,10] due to the adsorption of hydrophilic $Mg(OH)_2$ precipitates on the mineral surface [11,12].

Many investigators have attempted to relieve or even eliminate the detrimental effects of seawater in the mineral flotation process by adding chemical reagents. For instance, Jeldres et al. [1] found that the addition of $CaO-Na_2CO_3$ mixtures into pulp could remove

inevitable cations from seawater, thereby increasing mineral recovery. Li et al. [13] and Peng et al. [6] reported that the common dispersants; e.g., sodium hexametaphosphate (SHMP) and sodium silicate (SS), had a significantly positive role in reducing the adsorption of positively charged hydrophilic seawater precipitation (i.e., $Mg(OH)_{2(S)}$) on the negatively charged surfaces of sulfide minerals.

Kerosene emulsion, such as that using n-paraffines, iso-paraffines, naphthalene, and aromatics [14], a widely used collector in mineral flotation [7,15], was also applied as a modifier to improve mineral recovery in seawater. For instance, Suyantara et al. [12] investigated the effects of emulsified kerosene on chalcopyrite flotation in artificial seawater at pH 10, and found that chalcopyrite recovery increased from 20% to 30% with an increasing concentration of kerosene from 0 to 416 mg/L. Hirajima et al. [11] reported a positive role of kerosene on chalcopyrite flotation at pH 11. However, the influencing mechanism of kerosene emulsion on chalcopyrite flotation in seawater is still unclear, especially in the interactions among kerosene emulsion, chalcopyrite, and precipitate. Therefore, it is necessary to systematically investigate the effects of kerosene emulsion on chalcopyrite flotation in seawater flotation system.

Generally, the aggregation/dispersion behavior among minerals and neutral oils in the flotation process can be revealed by the extended Derjaguin–Landau–Verwey–Overbeek (EDLVO) theory via calculating the interaction energy as a function of separation distance, in which the van der Waals interaction, electrostatic interaction, and hydrophobic/hydrophilic force interaction are commonly involved and formulated [16–19]. In addition, density functional theory (DFT), a quantum mechanical method, was applied widely to investigate the adsorption mechanism of reagents on mineral surface [20–23]. However, less attention has been paid to the application of DFT in mineral flotation using seawater in the presence of kerosene.

In this study, the role of kerosene emulsion on chalcopyrite floatability in the presence of 0.05 M $MgCl_2$ (comparable to the representative Mg^{2+} concentration in seawater) was systematically investigated in the presence of kerosene emulsion. The influencing mechanisms were studied in detail via various measurements such as contact angle, zeta potential, and scanning electron microscopy (SEM). In addition, the theoretical calculations using EDLVO and DFT were also investigated. This study therefore provides a strategy to relieve the negative influence of seawater on chalcopyrite flotation.

2. Materials and Methods

2.1. Materials

The chalcopyrite sample, purchased from GEO Discoveries, Australia, was crushed, ground, and wet-sieved sequentially, and a size fraction of 38~75 μm was selected. Subsequently, the obtained chalcopyrite sample was treated by sonication in ethanol (analytically pure) to remove clinging fines. The powder sample was then freeze-dried over 24 h prior to storing in plastic tubes sealed under N_2 atmosphere (99.99% purity). These tubes were then placed in a -20 °C freezer to minimize surface oxidation. The purity of the chalcopyrite sample was greater than 90%, based on the chemical analysis our previous study reported [9].

Millipore pure water (Billerica, MA, USA) with a resistivity of 18.2 MΩ·cm was used in flotation and sample analysis when required. Kerosene ($C_{12}H_{26}$ and $C_{12}H_{18}$, Hubei Liwei Oil Products Sales Co., Ltd, Hanchuan, China) was used as the collector and was of technical grade; while other reagents used, including the TX-10P emulsifier ($C_{32}H_{58}O_{10}$, Hubei Xinrunde Chemical Co., Ltd, Wuhan, China) and the sodium hydroxide pH adjuster (NaOH, Sinopharm Group Co., Ltd., Beijing, China), were of analytical grade. In each given emulsification test, 5 mL of kerosene, 0.4 mL of TX-10P emulsifier, and 35 mL of pure water were mixed in a 100 mL beaker and then placed in an ultrasound device (LP-XP1000, Laipu, Wuxi, China). After ultrasonic treatment for 3 min and an interval of 1 s, the kerosene emulsion was obtained.

2.2. Flotation Experiments

Chalcopyrite flotation experiments were conducted using a hanging-trough-type flotation machine (XFG II, Wuhan Exploration Machinery Factory, Wuhan, China) at 1200 rpm. A total of 1 g of chalcopyrite powders (38~75 µm) was added into 25 mL pure water or 0.05 M $MgCl_2$ solution, while adjusting and maintaining the pulp at pH = 10 within 6 min, using 0.1 M NaOH solution. The kerosene emulsion was then added and stirred for another 6 min. Subsequently, flotation concentrates were collected every 10 s with an airflow rate of 1.2 cm·s^{-1} within 10 min. Both the floated and tailing fractions were filtered, rinsed three times using pure water to remove the residue from the chalcopyrite's surface, and then dried at 70 °C for 2 h prior to weighing.

2.3. Contact Angle Measurements

The sessile drop technique was applied to measure the contact angle of the chalcopyrite slab using a JC2000C1 goniometer (Shanghai Zhongchen Digital Technology Company, China). A chalcopyrite slab (2 cm × 2 cm × 2 cm) from the same source as the flotation experiment was progressively polished using 2000- and 5000-grit metallographic abrasive papers. Prior to contact angle measurements, the chalcopyrite slab was immersed into the same conditioned solution as used in the flotation test for 10 min. The treated slab was then softly rinsed three times using pure water and finally air-dried. After a water drop (0.25 µL) was placed onto the chalcopyrite slab surface using a microsyringe, the formed drop profile was captured and measured as the contact angle. Each test was performed three times, and the average value was reported.

2.4. Zeta Potential Measurements

A Zetasizer Nano-zs90 (Malvern Co., Ltd., Malvern, UK) was applied to measure the zeta potential. A total of 0.05 g of chalcopyrite powders (<5 µm) was added into 50 mL pure water or 0.05 M $MgCl_2$ solution. Kerosene emulsion was added into the suspension, and subsequently pH was adjusted and maintained at 10 for 10 min. The suspension was then transferred to a sample vessel for zeta potential measurements at 25 ± 1 °C. Each experiment was repeated at least thrice with a typical variation of ±5 mV in the zeta potential, and finally the average value was reported. The zeta potential measurements for the precipitates observed in 0.05 M $MgCl_2$ solution were conducted in a similar way as those for the mineral samples. For zeta potential of pure kerosene droplets, a 50 mL solution with 400 ppm kerosene emulsion was adjusted to pH 10 and measured. The pH adjustment and measurement processes were similar to that of chalcopyrite.

2.5. Solution Chemistry

Solution chemistry in 0.05 M $MgCl_2$ solution was calculated over pH 7~12 using the Origin software. The reactions and equilibrium constants of magnesium species involved in Li et al. [8] were used in this study.

2.6. Microscopic Measurements

A Sunny CX40P optical microscope equipped with a digital camera (Ningbo Sunny Instrument Co., Ltd., Ningbo, China) was used to investigate the adsorption morphologies of the $Mg(OH)_2$ precipitate and kerosene emulsion on the chalcopyrite's surface. A suspension droplet containing chalcopyrite particles (38~75 µm), $Mg(OH)_2$ precipitates, or kerosene emulsion was placed onto a clean glass plate and then covered with a thin glass slide to fix the suspension. The adsorption morphologies of precipitate and emulsion on the chalcopyrite was then photographed.

2.7. SEM-EDS Measurements

The untreated sample and samples prepared by the same flotation procedure were analyzed by scanning electron microscope (SEM, JSM-5610LV, JEOL Inc, Tokyo, Japan) equipped with a Phoenix energy-dispersive spectroscopy detector (EDS, EDAX Inc, Philadel-

phia, PA, USA). For this work, the accelerating voltage and vacuum mode resolution of the SEM were 15 kV and 4.0 nm, respectively. Before the test, the conditioned sample was dried in a vacuum freeze-dryer, prior to analysis.

2.8. Particle Size Measurement

The size of the chalcopyrite power (38~75um) used in this study was obtained by using −200 and +400 mesh vibrating screens (Shangyu Huafeng Hardware Instrument Co., LTD, Shaoxing, China). The sample sizes including chalcopyrite, precipitates formed in $MgCl_2$ solutions, and kerosene in the solution were measured with a BT-9300S laser particle size analyzer (Dandong Best Instrument Co., LTD, Dandong, China).

2.9. Theoretical Calculation

2.9.1. Extended DLVO Theory

The classic DLVO theory, a quantitative theory of the stability in aggregations or dispersions of charged particles [24], can be considered to explain the heterocoagulation behavior between particles in flotation process. However, this theory only involves the van der Waals energy V_w and the electrostatic interaction energy V_e, which is, not appropriately applied when the natural or induced particle surfaces are very hydrophobic (or hydrophilic), where the contact angle of particles is greater than 40° or less than 20° [24–27]. This is mainly due to the presence of hydrophobic interaction energy, which is an attractive structural component in an aqueous medium, and usually is observed in the range from 2 to 32 nm [27,28].

In previous studies, the extended DLVO (EDLVO) theory involved the hydrophobic interaction energy V_h, in addition to V_w and V_e, which was reported to explain the hydrophobic aggregation of particles in the flotation process, including particles or particle–oil systems [25,26,29,30]. For instance, Li et al. [25] studied the interaction energies V_w, V_e, and V_h between fine and coarse hematite particles (the natural contact angle was about 20°, and the contact angle treated by the NaOL collector was about 107°) in an aqueous suspension. Li et al. [26] calculated these three interaction energies between a kerosene droplet (one nonpolar oil)–hematite in a flotation process. In addition, many studies indicated that the pure chalcopyrite was naturally hydrophobic minerals, but the $Mg(OH)_2$ precipitate formed in $MgCl_2$ solution was hydrophilic [11,12,18,31]. Hence, the EDLVO theory was applied in a chalcopyrite/$Mg(OH)_2$–kerosene system herein to investigate the force between the kerosene droplet and particles presented in the aqueous flotation solution.

The adsorption or heterocoagulation between particles can be explained using the total potential energy (V_{total}) based on the EDLVO theory (Equation (1)) [19,25–27]:

$$V_{total} = V_w + V_e + V_h \tag{1}$$

V_w, V_e, and V_h can be calculated according to Equations (2)–(7) [19,32]:

$$V_w = -\frac{A}{6H}\left(\frac{R_1 R_2}{R_1 + R_2}\right) \tag{2}$$

$$A = (\sqrt{A_{11}} - \sqrt{A_{33}})(\sqrt{A_{22}} - \sqrt{A_{33}}) \tag{3}$$

$$V_e = \frac{\pi \varepsilon_0 \varepsilon_r R_1 R_2}{(R_1 + R_2)}\left(\psi_1{}^2 + \psi_2{}^2\right) \cdot \left\{\frac{2\psi_1 \psi_2}{\psi_1{}^2 + \psi_2{}^2}\cdot ln\left[\frac{1 + exp(-\kappa H)}{1 - exp(-\kappa H)}\right] + ln[1 - exp(-2\kappa H)]\right\} \tag{4}$$

$$V_h = -\frac{K}{6H}\left(\frac{R_1 R_2}{R_1 + R_2}\right) \tag{5}$$

$$K = \sqrt{K_1 K_2} \tag{6}$$

$$logK_{1(2)} = -3.194cos\theta - 18.229 \tag{7}$$

where R is the radius of particles/droplets (e.g., chalcopyrite, $Mg(OH)_2$ and kerosene emulsion). According to the particle size analysis, the average diameter (d_{50}) of the chalcopyrite particles was approximately 70 μm, while that of the formed $Mg(OH)_2$ precipitate was about 7.6 μm. Therefore, the

average radii of chalcopyrite particles and the Mg(OH)$_2$ precipitate in a 0.05 M MgCl$_2$ solution could be considered as 35.0 μm and 3.8 μm, respectively. The d$_{50}$ of kerosene emulsion was determined to be approximately 2.6 μm. Therefore, the radius of the kerosene emulsion was 1.3 μm. *H* is the distance between particles. *A* is the effective Hamaker constant for particle/water/particle, calculated based on Equation (3). The Hamaker constant *A* of chalcopyrite, kerosene, and Mg(OH)$_2$ was 3.25×10^{-20} J [16], 7.7×10^{-20} J [17], and 1.62×10^{-20} J [33], respectively. The Hamaker constant of water A_{33} was 3.7×10^{-20} J [34]. ε_0 and ε_r are the vacuum dielectric constant and water relative dielectric constant, and their product was 6.95×10^{-10} C^2/(J·m) [35]. κ^{-1} is the Debye length, and $\kappa = 0.18$ nm^{-1} [19,36,37]. ψ is the surface potentials (mV) of particles or droplets, usually represented by the zeta potential. *K* is the hydrophobic parameter between particles in aqueous solution [27], while K_1 or K_2 are the hydrophobic parameters of single chalcopyrite or Mg(OH)$_2$ particles, which can be assessed by Equation (7) [26]. Herein, *θ* is the contact angle of particles [27].The hydrophobic parameter of kerosene emulsion was 6.0×10^{-18} J [38].

2.9.2. DFT Calculation

Density functional theory (DFT) calculation was performed using the CASTAP module with a PW91 generalized gradient approximation (GGA) [39]. The interaction potential between valence electrons and ions was approximated using the ultrasoft potential (USP) [40]. The integral calculation of the Brillouin area used $3 \times 3 \times 3$ for geometric optimization and a $3 \times 3 \times 1$ Monkhorst–Pack k-point network [41] for electronic structure calculation.

Kerosene is mainly composed of alkanes and aromatic hydrocarbons with 8~16 carbon atoms, in which the typical linear paraffins in kerosene are dodecane (n-C$_{12}$H$_{26}$), while the aromatic hydrocarbons of kerosene usually carry one benzene ring ($-$C$_6$H$_5$) [14,42]. Therefore, the straight-chain paraffin (C$_{12}$H$_{26}$) and straight-chain aromatic hydrocarbons (C$_{12}$H$_{18}$) were selected as two representative components of kerosene. In addition, previous studies have shown that the chalcopyrite (112) surface is the main crystal face [20]. Therefore, in the D

FT calculation process, C$_{12}$H$_{26}$/C$_{12}$H$_{18}$ and Mg(OH)$_2$ were selected and built in the same box to calculate the adsorption energies (ΔE) on chalcopyrite (112) surface using Equation (8) [43]:

$$\Delta E = E_{surf+ads} - E_{surf} - E_{ads} \tag{8}$$

where $E_{surf+ads}$, E_{surf}, and E_{ads} correspond to the energies of the whole system after adsorption, reconstructed surface, and adsorbate, respectively.

3. Results and Discussion

3.1. Flotation Experiment

As previous studies showed that the pulp pH in sulfide flotation separation was usually adjusted to 9.5~12 to depress pyrite flotation [1,11,44]; therefore, a pH of 10 was applied in this study, which was similar to other investigations [9,45–47].

Figure 1 shows the effect of kerosene emulsion on chalcopyrite flotation recovery with and without 0.05 M MgCl$_2$ solution at pH 10. In pure water, a flotation recovery of 68.1% was obtained in the absence of kerosene emulsion, indicating a good natural floatability of chalcopyrite [9]. An increment of approximately 24% to approximately 90% for chalcopyrite recovery was found when 200 ppm kerosene emulsion was added. However, an insignificant increase was found with further addition of kerosene emulsion up to 400 ppm. A recovery of 14.8% was obtained in 0.05 M MgCl$_2$ in the absence of kerosene, indicating that the presence of Mg^{2+} significantly inhibited chalcopyrite flotation under an alkaline condition (i.e., pH = 10), consistent with previous studies [6,12,13]. Differently, chalcopyrite flotation recovery increased gradually from 15.4% to 40% with increasing kerosene emulsion dosage from 100 to 400 ppm, suggesting the beneficial role of kerosene emulsion.
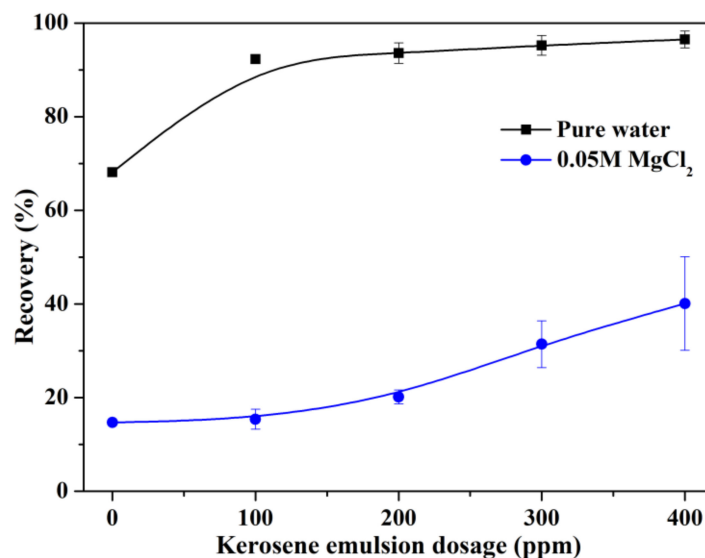
Figure 1. Chalcopyrite recovery as a function of kerosene emulsion dosage, at pH 10.

3.2. Contact Angle Analyses

Figure 2 shows the contact angle of the chalcopyrite's surface exposed to various dosages of kerosene emulsion in pure water and 0.05 M MgCl$_2$ solution at pH 10. The contact angle of freshly polished chalcopyrite immersed in pure water was approximately 63.3°, close to that reported previously [9,11], indicating a good hydrophobicity of the natural chalcopyrite. The contact angle was increased linearly to 81.8° with increasing kerosene emulsion concentration from 100 to 400 ppm, suggesting a positive role of kerosene emulsion in chalcopyrite hydrophobicity. However, chalcopyrite flotation recovery increased insignificantly when kerosene emulsion was greater than 200 ppm (Figure 2), indicating that the later addition of 200 ppm kerosene emulsion only increased the chalcopyrite's hydrophobicity, rather than the flotation recovery. These results confirmed that kerosene emulsion promoted chalcopyrite floatability by increasing its hydrophobicity, most likely via forming a thin hydrophobic layer on the chalcopyrite's surface [48].
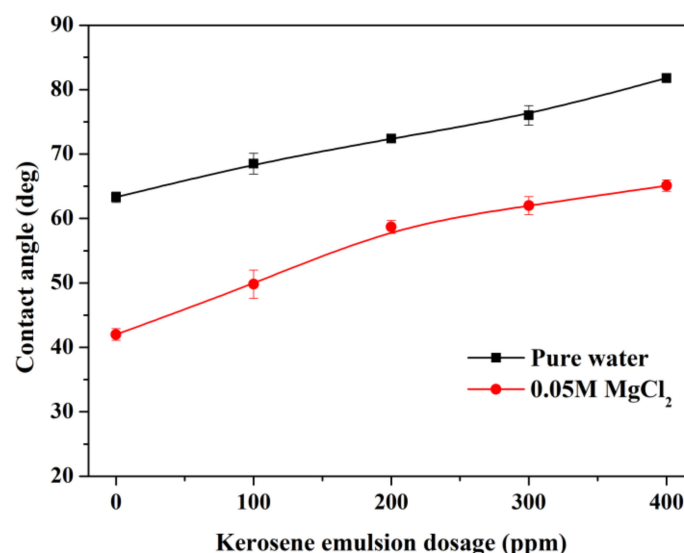

Figure 2. Contact angles of the chalcopyrite's surface in pure water and 0.05 M MgCl$_2$ solution at pH 10, as a function of kerosene emulsion dosage.

In the absence of kerosene, the contact angle of the chalcopyrite's surface treated in 0.05 M MgCl$_2$ solution was measured at approximately 42.0°, lower than that in pure water, but similar to that reported by Li et al. [18] and Suyantara et al. [12], further indicating that the presence of MgCl$_2$

greatly decreased the chalcopyrite's hydrophobicity, possibly due to the adsorption of hydrophilic species (i.e., $Mg(OH)_{2(S)}$) formed on the chalcopyrite's surface.

A gradual increase in contact angle was observed in 0.05 M $MgCl_2$ solution when increasing the kerosene emulsion dosage, achieving 65.1° in the presence of 400 ppm kerosene emulsion. This indicated that kerosene was beneficial to decreasing the surface wettability of the chalcopyrite, thereby improving its flotation recovery. It should also be noted that the increment of the chalcopyrite contact angle in the range of 0~200 ppm kerosene emulsion was slightly greater than that of the 200~400 ppm kerosene emulsion (0.0835°/ppm vs. 0.032°/ppm), while the increment of chalcopyrite flotation recovery due to the initial 200 ppm kerosene addition was lower than that due to the later 200 ppm kerosene addition (0.0274%/ppm vs. 0.0996%/ppm). These results illustrated that initial addition of kerosene emulsion may play another role in chalcopyrite flotation in 0.05 M $MgCl_2$ solution. For example, the initial kerosene added in solution may prevent the adsorption of hydrophilic species onto the chalcopyrite's surface.

3.3. Solution Chemistry

Mg^{2+} in solution can hydrolyze into various Mg-containing species at different pHs. These Mg-containing species may affect the surface properties of minerals and the flotation recovery [1,6,12,13,49]. As shown in Figure 3, the Mg^{2+}, $MgOH^+$, $Mg(OH)_{2(aq)}$, and $Mg(OH)_{2(s)}$ were the most probable Mg-containing species formed in 0.05 M $MgCl_2$ solution when pH > 9.3. Specifically, when pH was 10 (flotation pH herein), about 0.048 M Mg precipitation ($Mg(OH)_{2(s)}$) was formed in solution, accounting for 96% of the total Mg species (0.05M). Previous studies indicated that $Mg(OH)_{2(s)}$ produced in 0.05 M $MgCl_2$ solution could be adsorbed on the surface of sulfide minerals by a "slime coating" mechanism [1,6,12,13,49], further reducing the recovery. Therefore, the depressed chalcopyrite recovery was more likely relevant to the formation and adsorption of hydrophilic $Mg(OH)_2$ precipitates onto the chalcopyrite's surface.
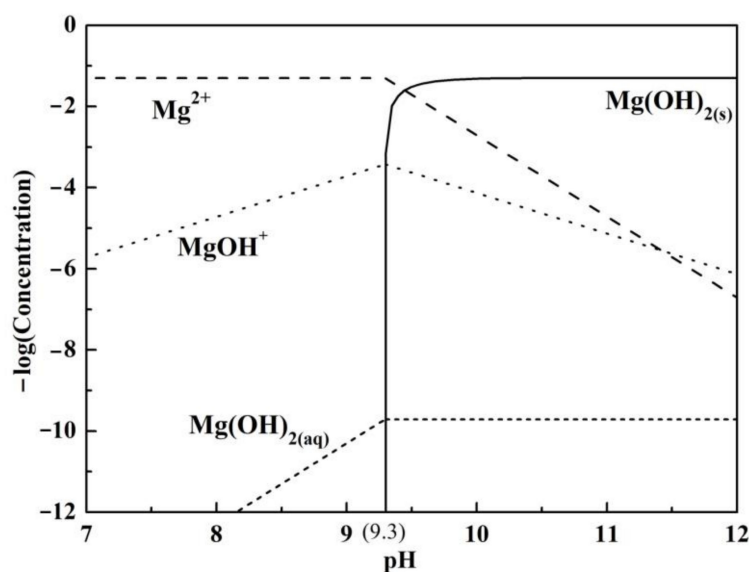

Figure 3. Solution species in 0.05 M $MgCl_2$ solution.

3.4. Microscopic Analyses

Figure 4 shows the optical images of suspension in various solutions controlled at pH 10. Different from the small kerosene emulsion droplets in pure water (Figure 4a), a large amount of irregular colloidal precipitation attributed to formed $Mg(OH)_2$ colloids (Li et al., 2017) appeared in 0.05 M $MgCl_2$ solution (Figure 4b). Figure 4c shows that the formed $Mg(OH)_2$ precipitates in 0.05 M $MgCl_2$ solution surrounded the chalcopyrite particles, which may have reduced surface hydrophobicity and the floatability of the chalcopyrite. In previous studies, Hirajima et al. [11] found the formation of Mg precipitates on the chalcopyrite's surface treated in $MgCl_2$ solution using AFM measurement, while Li et al. [13] reported the adsorption of $Mg(OH)_2$ precipitates on the chalcopyrite's surface in $MgCl_2$ solution by XPS analysis. These studies supported the formation and adsorption of $Mg(OH)_2$ precipitates on the chalcopyrite's surface.
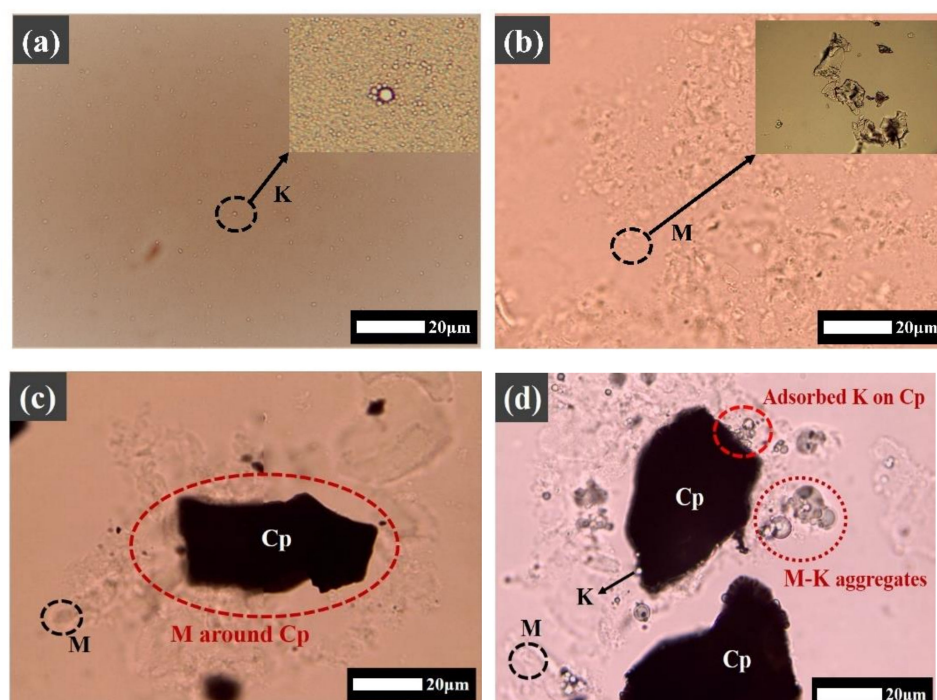
Figure 4. Optical images of: (**a**) kerosene emulsion; (**b**) precipitates in 0.05 M MgCl$_2$; (**c**) chalcopyrite in 0.05 M MgCl$_2$; (**d**) chalcopyrite + kerosene in 0.05 M MgCl$_2$. All solutions were controlled at pH 10. Cp—chalcopyrite; M—Mg(OH)$_2$; K—kerosene droplet.

However, significantly fewer Mg(OH)$_2$ precipitates presented on the chalcopyrite's surface when 400 ppm kerosene emulsion was added (Figure 4d). Instead, many Mg(OH)$_2$—kerosene emulsion aggregates were found, indicating the beneficial roles of kerosene emulsion on enhancing chalcopyrite flotation recovery, probably via decreasing the adsorption of hydrophilic Mg(OH)$_2$ on the chalcopyrite's surface. In addition, it should be noted that the flotation of pure Mg(OH)$_2$ in the presence of kerosene can be negligible, due possibly to its small size (i.e., R = 3.8 µm; see Section 2.9.1).

3.5. SEM-EDS Analyses

In order to further understand the evolution of the chalcopyrite's surface composition, SEM measurements were taken. Figure 5a shows that the untreated chalcopyrite surface was relatively smooth and clean. EDS analyses (Table 1) further indicated that the untreated chalcopyrite surface presented a small amount of O (1.4 wt %), in addition to the major elements of Cu, Fe, and S due to slight oxidation [18], without other impurities being found. In contrast, the chalcopyrite surface treated in 0.05 M MgCl$_2$ solution was significantly rougher (Figure 5b), with O content being sharply increased from 1.4 wt % to 8.1 wt %. In addition, a 4.1 wt % Mg content was found (Table 1), suggesting the adsorption of Mg-containing substance on the chalcopyrite's surface. It should be noted that the addition of kerosene emulsion significantly reduced the O and Mg concentrations on the chalcopyrite's surface exposed to 0.05 M MgCl$_2$ solution; e.g., from 8.1 wt % and 4.1 wt % to 3.2 wt % and 1.0 wt %, respectively, suggesting that kerosene emulsion could reduce the adsorption of Mg(OH)$_2$, consistent with the results shown in Figure 4. This also supported our findings of the beneficial roles of kerosene emulsion on chalcopyrite flotation in 0.05 M MgCl$_2$ solution.
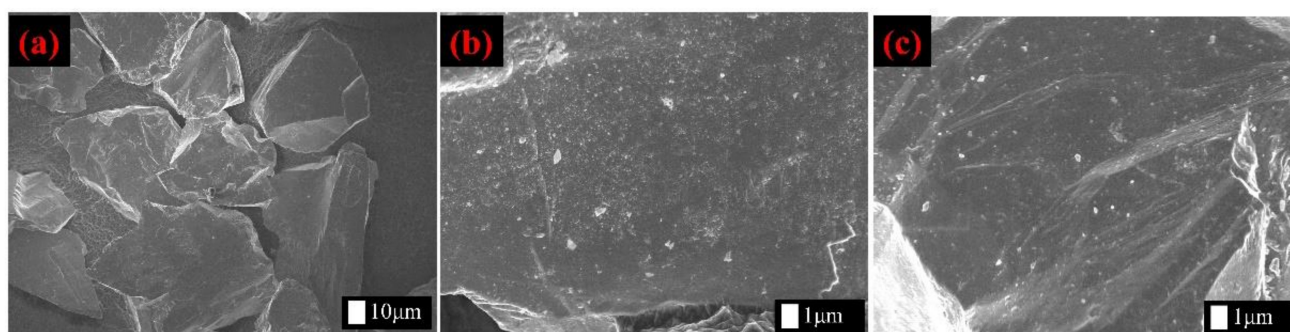
Figure 5. SEM images of chalcopyrite surfaces under different conditions: (**a**) untreated chal- copyrite; (**b**) chalcopyrite treated in 0.05 M MgCl$_2$ solution at pH 10; (**c**) 0.05M MgCl$_2$ + 400 ppm kerosene solution at pH 10.

Table 1. Elemental composition (wt %) of chalcopyrite surface under different conditions.

Element	Untreated	MgCl$_2$	MgCl$_2$ + Kerosene
Cu	35.5	26.3	31.7
Fe	30.9	32	32.1
S	32.2	29.5	32
O	1.4	8.1	3.2
Mg	/	4.1	1
Total	100	100	100

3.6. Mechanisms

3.6.1. Influence of Kerosene Emulsion Dosage

In order to further investigate the influencing mechanisms of kerosene emulsion dosage on the chalcopyrite's surface, the contact angles shown in Figure 2 were fitted and presented in Figure 6, in which one linear trend and good regression (correlation coefficient R^2 > 0.99) were obtained in pure water, suggesting that the increasing hydrophobicity of chalcopyrite was linearly corrected to the kerosene emulsion dosage (0.04583°/ppm) in the absence of MgCl$_2$. However, the evolution of the contact angle in 0.05 M MgCl$_2$ solution was present in a nonlinear trend, within 400 ppm kerosene emulsion. In contrast, two fitted lines with R^2 greater than 0.999 were observed, indicating two influencing mechanisms due to the presence of kerosene emulsion. For instance, when kerosene emulsion dosage was lower than 200 ppm, the increasing rate of contact angle was 0.08345°/ppm, while its rate was decreased to 0.03198°/ppm when the kerosene emulsion dosage was in the range of 200~400 ppm.
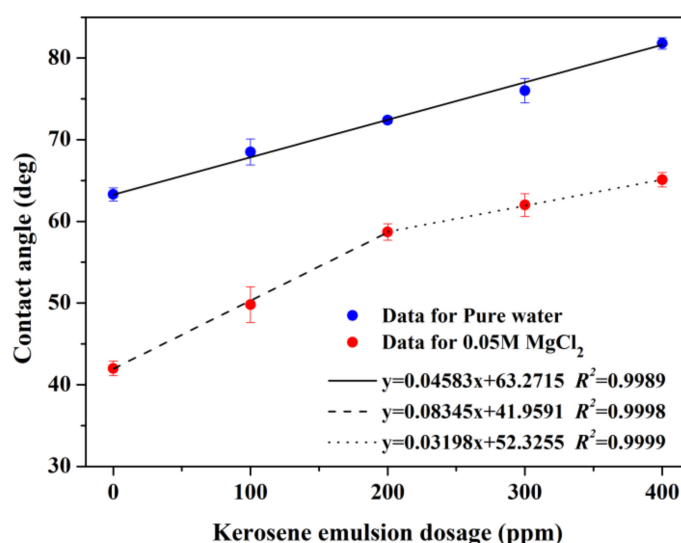

Figure 6. Contact angles of chalcopyrite surface as a function of kerosene emulsion dosage.

As discussed in Figures 3 and 4, a mass of hydrophilic Mg(OH)$_2$ precipitates were formed and adsorbed on the chalcopyrite's surface in 0.05 M MgCl$_2$ solution, lowering its hydrophobicity. When kerosene emulsion was added in the flotation process, the kerosene drop not only adsorbed on the chalcopyrite's surface, but also formed kerosene-Mg(OH)$_2$ aggregates (Figure 4d), reducing the attachment of Mg(OH)$_2$ onto the chalcopyrite's surface. Therefore, the possible mechanisms of kerosene emulsion dosage on the chalcopyrite's surface in 0.05M MgCl$_2$ solution were proposed herein. Firstly, when the kerosene emulsion dosage was lower than 200 ppm, the kerosene drop was preferentially attached to Mg(OH)$_2$ precipitants, forming kerosene-Mg(OH)$_2$ aggregates and reducing the adsorption of Mg(OH)$_2$ onto the chalcopyrite's surface. This also resulted in a rapid increase in the contact angle. When the kerosene emulsion dosage was adequate (>200 ppm), the surplus kerosene drops could be adsorbed onto the chalcopyrite's surface, increasing its hydrophobicity. In order to further understand the interaction among chalcopyrite, Mg(OH)$_2$, and kerosene, the zeta potential analyses and EDLVO theory calculation were carried out.

3.6.2. Zeta Potential Analyses and EDLVO Theory Calculation

Figure 7 shows the zeta potentials of the chalcopyrite particles and Mg(OH)$_2$ precipitates in the presence of kerosene emulsion in pure water at pH 10. A zeta potential of -30.27 mV and -80.73 mV was found for chalcopyrite particles and kerosene, respectively, indicating that both the chalcopyrite's surface and kerosene were negatively charged. With increasing kerosene concentration from 100 to 400 ppm, the zeta potential of chalcopyrite in pure water decreased linearly; e.g., from -35.1 mV to -40.3 mV, possibly due to the adsorption of more negatively charged kerosene onto the chalcopyrite's surface [17].
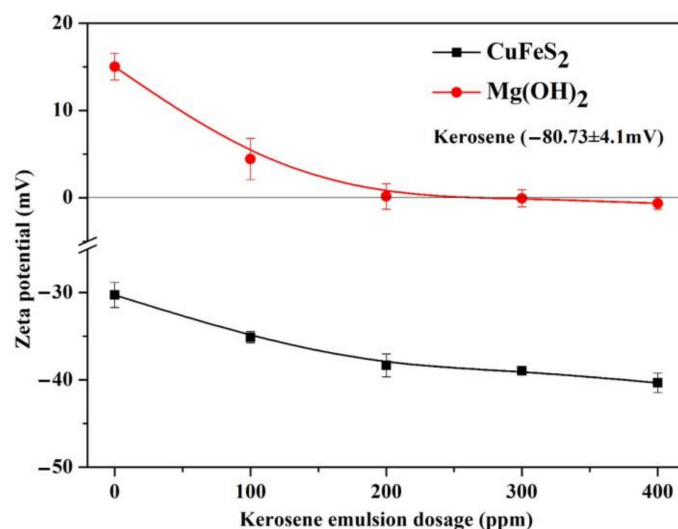

Figure 7. Zeta potentials of chalcopyrite particles and Mg(OH)$_2$ precipitates as a function of kerosene dosage in pure water, controlled at pH 10.

A positive zeta potential of about 15 mV was observed for Mg(OH)$_2$ precipitates in the absence of kerosene emulsion in pure water, close to that reported in previous studies [18,50]. When the kerosene emulsion was increased from 0 to 200 ppm, the zeta potential dropped significantly to 0.14 mV. When further increasing the kerosene emulsion concentration from 200 to 400 ppm, the zeta potential decreased slightly, and even reversed to a negative value (about -0.64 mV), illustrating that the addition of negatively charged kerosene emulsion changed the surface electrical property of the positively charged Mg(OH)$_2$ from positive to negative. Suyantara et al. [12] also reported that a kerosene emulsion with electronegativity was more easily adsorbed on formed Mg(OH)$_2$ precipitates than a positively charged one.

As discussed above, chalcopyrite flotation behaviors herein were strongly connected with Mg(OH)$_2$ precipitates and kerosene emulsion, which usually can be explained by the interaction between particles [6,13,35]. Therefore, the interaction energies of V_w, V_e, and V_h and V_{total} among chalcopyrite, kerosene, and Mg(OH)$_2$ were calculated, and are presented in Figure 8.
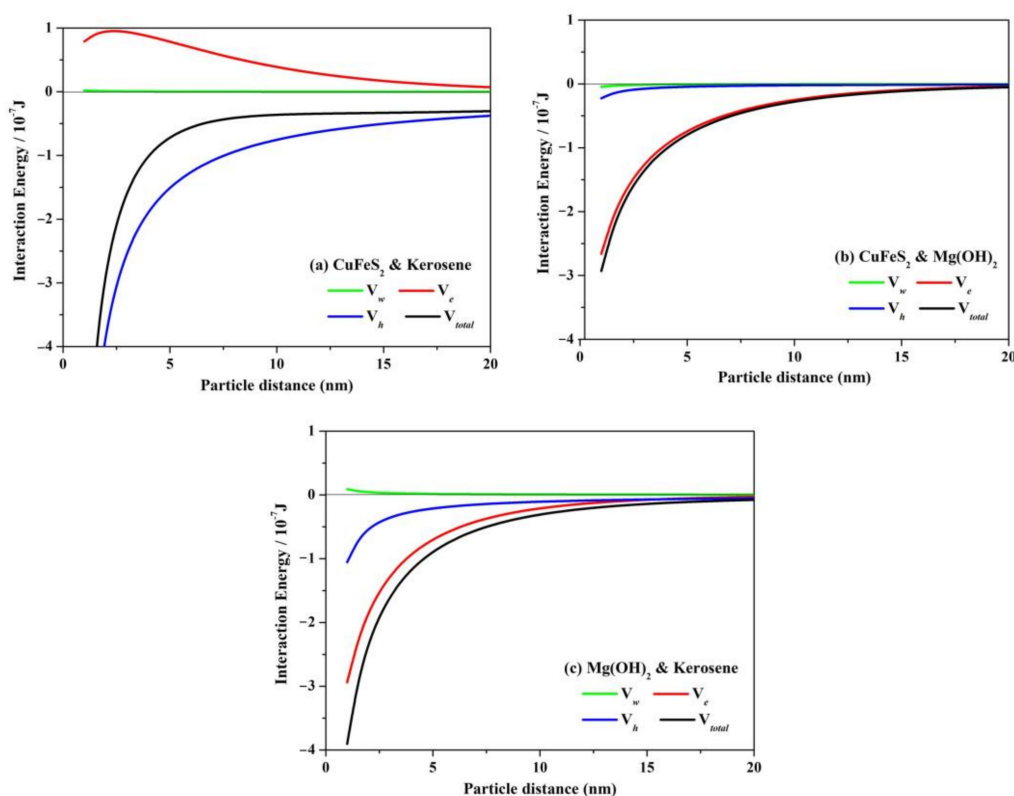
Figure 8. Interaction energy as a function of distance between (**a**) chalcopyrite and kerosene, (**b**) chalcopyrite and Mg(OH)$_2$, and (**c**) Mg(OH)$_2$ and kerosene at pH = 10, in pure water.

Figure 8 shows a very small V_w among chalcopyrite particles, kerosene, and Mg(OH)$_2$, compared to V_e and V_h. For instance, as shown in Table 2, when the distance was 2 nm, the V_w among chalcopyrite, kerosene, and Mg(OH)$_2$ were about 10^{-9} J; while the V_e and V_h among chalcopyrite, kerosene, and Mg(OH)$_2$ ranged from 10^{-8} to 10^{-7} J, indicating that the V_w was 1~2 magnitudes smaller than those of V_e and V_h. This therefore suggested that the V_w was negligible in the flotation system. Li et al. [26] also found a lowest value of V_w compared to the V_e and V_h within a distance of 0~40 nm in hematite–kerosene flotation. Therefore, the V_w was not considered as the main force in this study.

Table 2. The interaction energies (10^{-7} J) among chalcopyrite, kerosene, and Mg(OH)$_2$ at a distance of 2 nm.

Particles	V_w	V_e	V_h	V_{total}
CuFeS$_2$ and Kerosene	0.01	0.95	−3.77	−2.81
CuFeS$_2$ and Mg(OH)$_2$	−0.02	−1.74	−0.11	−1.87
Mg(OH)$_2$ and Kerosene	0.04	−1.83	−0.53	−2.32

As shown in Figure 8a, the total interaction energy between chalcopyrite and kerosene was negative, and their main interaction energy was negative V_h, indicating that the adsorption of kerosene emulsion on the chalcopyrite's surface was mainly via a hydrophobicity attractive interaction force, thereby increasing the chalcopyrite's hydrophobicity and floatability. Figure 8b indicates that the V_{total} between chalcopyrite and Mg(OH)$_2$ was negative within all examined distances, suggesting that the attractive force dominated the interaction between the negatively charged chalcopyrite and positively charged Mg(OH)$_2$. In addition, the V_w, V_e, and V_h were negative, and the absolute value of V_e was greatest among three interaction energies, revealing that the attractive interaction between chalcopyrite and Mg(OH)$_2$ was mainly attributed to the strong electrostatic interaction. Therefore, the reduced hydrophobicity and floatability of chalcopyrite was primarily due to the adsorption of hydrophilic Mg(OH)$_2$.

Figure 8c shows the interaction force between $Mg(OH)_2$ and kerosene. The V_w showed a positive value, while the V_e and V_h presented negative values, eventually giving rise to a negative V_{total}. Specifically, the absolute value of V_e was significantly greater than that of V_h, indicating that the negative V_e played a dominant role in V_{total} between $Mg(OH)_2$ and kerosene. Thus, these two compounds were easily attached to each other, forming kerosene–$Mg(OH)_2$ aggregates.

3.6.3. DFT Calculation

Table 3 shows the adsorption energy calculated based on the DFT calculation. The adsorption energies of straight-chain paraffin and aromatic hydrocarbons (the main components of kerosene emulsion) on the chalcopyrite (112) surface were −447.48 and −401.19 kJ·mol^{-1}, while they were −500.52 kJ·mol^{-1} and −439.77 kJ·mol^{-1} for the $Mg(OH)_2$ surface, indicating that the kerosene emulsion could more easily attach onto the surfaces of the $Mg(OH)_2$ colloids, as compared to those of chalcopyrite particles, thereby resulting in an interaction order of kerosene and $Mg(OH)_2$ > kerosene and chalcopyrite > chalcopyrite and $Mg(OH)_2$. In other words, the kerosene emulsion was preferentially adsorbed with $Mg(OH)_2$ colloids, resulting in the formation of kerosene–$Mg(OH)_2$ aggregates (Figure 4), further preventing the adsorption of $Mg(OH)_2$ colloids on the chalcopyrite's surface, thereby improving the chalcopyrite flotation recovery.

Table 3. The adsorption energies (kJ·mol^{-1}) of various systems.

Adsorbate	Adsorbent	Adsorption Energies
Straight-chain paraffin ($C_{12}H_{26}$)	Chalcopyrite (112)	−447.48
Straight-chain aromatic hydrocarbon ($C_{12}H_{18}$)	Chalcopyrite (112)	−401.19
Straight-chain paraffin ($C_{12}H_{26}$)	$Mg(OH)_2$	−500.52
Straight-chain aromatic hydrocarbon ($C_{12}H_{18}$)	$Mg(OH)_2$	−439.77
$Mg(OH)_2$	Chalcopyrite (112)	−243.99

Figure 9 shows the electron density of the main components of the kerosene emulsion or $Mg(OH)_2$ molecule adsorbed onto the chalcopyrite (112) surface, in addition to the main components of the kerosene emulsion onto the $Mg(OH)_2$. No new bonds were formed on the chalcopyrite (112) surface for straight-chain paraffin/aromatic hydrocarbons (Figure 9a,b), indicating that no chemical reactions occurred between the kerosene emulsion and the chalcopyrite's surface. In other words, the kerosene emulsion was physically adsorbed onto the chalcopyrite (112) surface, and the hydrophobicity of the chalcopyrite enhanced by kerosene was due to the physical adsorption of kerosene [48]. Furthermore, the closest distances between chalcopyrite and kerosene, chalcopyrite and $Mg(OH)_2$, and $Mg(OH)_2$ and kerosene were 2.614 Å, 2.758 Å, and 2.599/2.550 Å, respectively, showing an distance order of $Mg(OH)_2$ and kerosene > chalcopyrite and kerosene > chalcopyrite and $Mg(OH)_2$. This further suggested that kerosene was more readily adsorbed with $Mg(OH)_2$ colloids. In contrast, the weakest adsorption occurred between chalcopyrite and $Mg(OH)_2$.

In order to further understand the interaction between the chalcopyrite, kerosene emulsion, and $Mg(OH)_2$, projected density of states (PDOS) analyses were carried out, and are shown in Figure 10. No obvious peak shift or overlap was found between the H 1s orbit from the straight-chain aromatic hydrocarbon and the O 2p orbit from $Mg(OH)_2$, before and after kerosene adsorption (Figure 10a vs. Figure 10f), indicating no strong chemical interaction between kerosene and $Mg(OH)_2$ [51]. A similar phenomenon was also observed between straight-chain paraffin and $Mg(OH)_2$, straight-chain aromatic hydrocarbon and chalcopyrite, straight-chain paraffin and chalcopyrite, and chalcopyrite and $Mg(OH)_2$, indicating no chemical bonds formed among kerosene, chalcopyrite, and $Mg(OH)_2$, consistent with the electron density results (Figure 9).
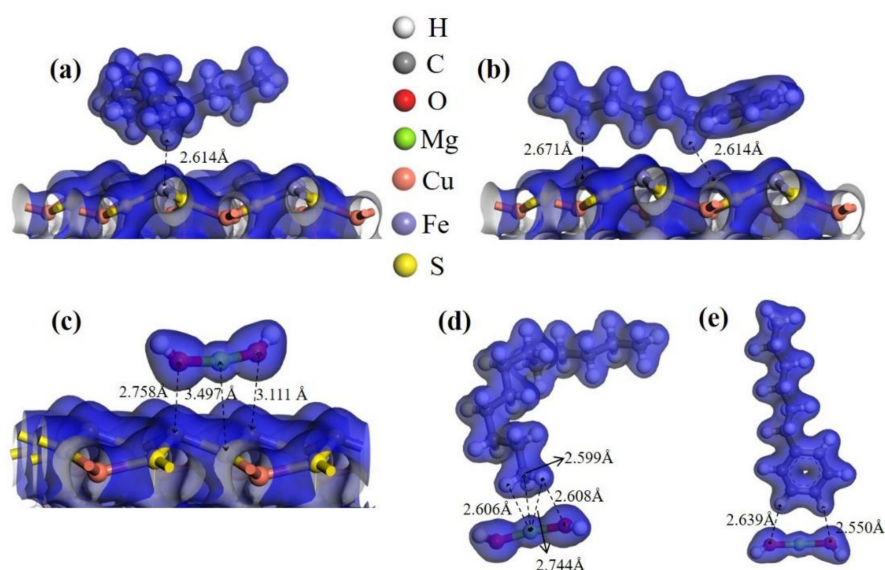
Figure 9. Electron density of (**a**) straight-chain paraffin, (**b**) straight-chain aromatic hydrocarbon, and (**c**) Mg(OH)$_2$ adsorbed on the chalcopyrite (112) surface; and electron density of (**d**) straight-chain paraffin and (**e**) straight-chain aromatic hydrocarbon on Mg(OH)$_2$.
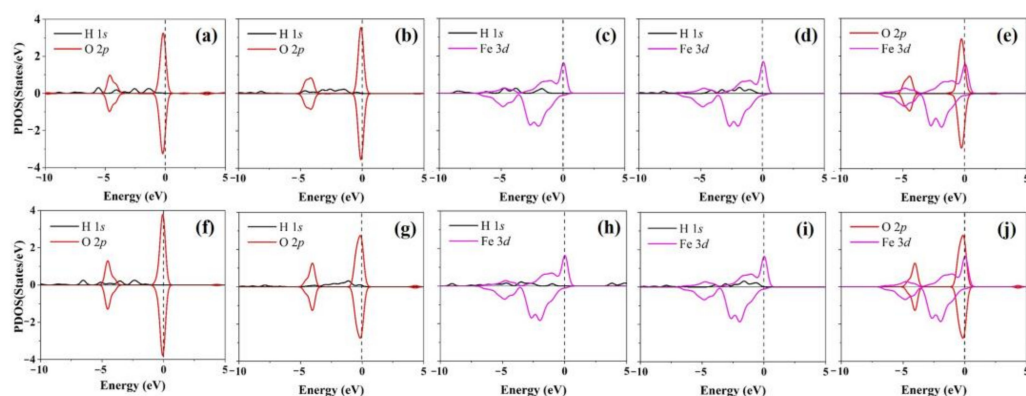

Figure 10. PDOS analysis of: (**a**,**f**) straight-chain aromatic hydrocarbon and Mg(OH)$_2$; (**b**,**g**) straight-chain paraffin and Mg(OH)$_2$; (**c**,**h**) straight-chain aromatic hydrocarbon and chalcopyrite; (**d**,**i**) straight-chain paraffin and chalcopyrite; (**e**,**j**) chalcopyrite and& Mg(OH)$_2$. (**a**–**e**) Before adsorption; (**f**,**j**) after adsorption.

4. Conclusions

The roles and influencing mechanisms of kerosene emulsion on chalcopyrite flotation in 0.05 M MgCl$_2$ solution were investigated by EDLVO and DFT approaches. Chalcopyrite recovery was significantly reduced in 0.05 M MgCl$_2$ solution at pH 10, mainly due to the formation and adsorption of Mg(OH)$_2$ precipitates onto the chalcopyrite's surface, increasing its hydrophilicity. The addition of kerosene emulsion was beneficial to recover the depressed chalcopyrite. The adsorption energies showed an order of kerosene and Mg(OH)$_2$ > kerosene and chalcopyrite > chalcopyrite and Mg(OH)$_2$. The main force between kerosene and Mg(OH)$_2$ was a strong electrostatic attraction interaction, while the predominant force between kerosene and chalcopyrite was a hydrophobicity attractive interaction. Herein, two beneficial mechanisms were proposed based on various measurements and theoretical calculations. Firstly, kerosene emulsion was preferentially adsorbed on Mg(OH)$_{2(s)}$ and formed kerosene–Mg(OH)$_2$ aggregates, further reducing the adsorption of Mg(OH)$_2$ on the chalcopyrite's surface. Secondly, an additional kerosene emulsion was attached onto the chalcopyrite's surface, forming hydrophobic agglomerates, and increasing surface hydrophobicity of the chalcopyrite, thereby promoting chalcopyrite floatability.

References

1. Jeldres, R.I.; Arancibia-Bravo, M.P.; Reyes, A.; Aguirre, C.E.; Cortes, L.; Cisternas, L.A. The impact of seawater with calcium and magnesium removal for the flotation of copper-molybdenum sulphide ores. *Miner. Eng.* **2017**, *109*, 10–13. [CrossRef]
2. Li, Y.; Kawashima, N.; Li, J.; Chandra, A.P.; Gerson, A.R. A review of the structure, and fundamental mechanisms and kinetics of the leaching of chalcopyrite. *Adv. Colloid Interface Sci.* **2013**, *197*, 1–32. [CrossRef]
3. Ikumapayi, F.; Rao, K.H. Recycling process water in complex sulfide ore flotation: Effect of calcium and sulfate on sulfide minerals recovery. *Miner. Process. Extr. Met. Rev.* **2014**, *36*, 45–64. [CrossRef]
4. Wang, B.; Peng, Y. The effect of saline water on mineral flotation—A critical review. *Miner. Eng.* **2014**, *66*, 13–24. [CrossRef]
5. Moreno, P.A.; Aral, H.; Cuevas, J.; Monardes, A.; Adaro, M.; Norgate, T.; Bruckard, W. The use of seawater as process water at Las Luces copper–molybdenum beneficiation plant in Taltal (Chile). *Miner. Eng.* **2011**, *24*, 852–858. [CrossRef]
6. Peng, Y.; Li, Y.; Li, W.; Fang, X.; Liu, C.; Fan, R. Elimination of adverse effects of seawater on molybdenite flotation using sodium silicate. *Miner. Eng.* **2019**, *146*, 106108. [CrossRef]
7. Suyantara, G.P.W.; Hirajima, T.; Elmahdy, A.M.; Miki, H.; Sasaki, K. Effect of kerosene emulsion in MgCl2 solution on the kinetics of bubble interactions with molybdenite and chalcopyrite. *Colloids Surf. A Physicochem. Eng. Asp.* **2016**, *501*, 98–113. [CrossRef]
8. Li, Y.; Li, W.; Wei, Z.; Xiao, Q.; Lartey, C.; Li, Y.; Song, S. The influence of common chlorides on the adsorption of SBX on chalcopyrite surface during flotation process. *Miner. Process. Extr. Met. Rev.* **2018**, *40*, 129–140. [CrossRef]
9. Li, Y.; Li, W.; Xiao, Q.; He, N.; Ren, Z.; Lartey, C.; Gerson, A.R. The influence of common monovalent and divalent chlorides on chalcopyrite flotation. *Minerals* **2017**, *7*, 111. [CrossRef]
10. Jeldres, R.I.; Forbes, L.; Cisternas, L.A. Effect of seawater on sulfide ore flotation: A review. *Miner. Process. Extr. Met. Rev.* **2016**, *37*, 369–384. [CrossRef]
11. Hirajima, T.; Suyantara, G.P.W.; Ichikawa, O.; Elmahdy, A.M.; Miki, H.; Sasaki, K. Effect of Mg^{2+} and Ca^{2+} as divalent seawater cations on the floatability of molybdenite and chalcopyrite. *Miner. Eng.* **2016**, *96–97*, 83–93. [CrossRef]
12. Suyantara, G.P.W.; Hirajima, T.; Miki, H.; Sasaki, K. Floatability of molybdenite and chalcopyrite in artificial seawater. *Miner. Eng.* **2018**, *115*, 117–130. [CrossRef]
13. Li, W.; Li, Y. Improved understanding of chalcopyrite flotation in seawater using sodium hexametaphosphate. *Miner. Eng.* **2019**, *134*, 269–274. [CrossRef]
14. Lissitsyna, K.; Huertas, S.; Quintero, L.; Polo, L. PIONA analysis of kerosene by comprehensive two-dimensional gas chromatography coupled to time of flight mass spectrometry. *Fuel* **2014**, *116*, 716–722. [CrossRef]
15. Liu, A.; Fan, M.-Q.; Fan, P.-P. Interaction mechanism of miscible DDA–Kerosene and fine quartz and its effect on the reverse flotation of magnetic separation concentrate. *Miner. Eng.* **2014**, *65*, 41–50. [CrossRef]
16. Sharma, P.; Rao, K.H. Adhesion of *Paenibacillus polymyxa* on chalcopyrite and pyrite: Surface thermodynamics and extended DLVO theory. *Colloids Surf. B Biointerfaces* **2003**, *29*, 21–38. [CrossRef]
17. Lin, Q.Q.; Gu, G.H.; Wang, H.; Liu, Y.C.; Fu, J.G.; Wang, C.Q. Flotation mechanisms of molybdenite fines by neutral oils. *Int. J. Miner. Metall. Mater.* **2018**, *25*, 1–10. [CrossRef]
18. Li, W.; Li, Y.; Xiao, Q.; Wei, Z.; Song, S. The influencing mechanisms of sodium hexametaphosphate on chalcopyrite flotation in the presence of MgCl2 and CaCl2. *Minerals* **2018**, *8*, 150. [CrossRef]
19. Yoon, R.H.; Mao, L. Application of extended DLVO theory, IV. *J. Colloid Interface Sci.* **1996**, *181*, 613–626. [CrossRef]
20. Wei, Z.; Li, Y.; Gao, H.; Zhu, Y.; Qian, G.; Yao, J. New insights into the surface relaxation and oxidation of chalcopyrite exposed to O_2 and H_2O: A first-principles DFT study. *Appl. Surf. Sci.* **2019**, *492*, 89–98. [CrossRef]
21. Li, L.; Zhang, C.; Yuan, Z.; Xu, X.; Song, Z. AFM and DFT study of depression of hematite in oleate-starch-hematite flotation system. *Appl. Surf. Sci.* **2019**, *480*, 749–758. [CrossRef]
22. Wang, Y.; Khoso, S.A.; Luo, X.; Tian, M. Understanding the depression mechanism of citric acid in sodium oleate flotation of Ca2+-activated quartz: Experimental and DFT study. *Miner. Eng.* **2019**, *140*, 105878. [CrossRef]
23. Li, Y.; Liu, Y.; Chen, J.; Zhao, C. Structure-activity of chelating collectors for flotation: A DFT study. *Miner. Eng.* **2020**, *146*, 106133. [CrossRef]
24. Yao, J.; Yin, W.; Gong, E. Depressing effect of fine hydrophilic particles on magnesite reverse flotation. *Int. J. Miner. Process.* **2016**, *149*, 84–93. [CrossRef]

25. Li, D.; Yin, W.; Liu, Q.; Cao, S.; Sun, Q.; Zhao, C.; Yao, J. Interactions between fine and coarse hematite particles in aqueous suspension and their implications for flotation. *Miner. Eng.* **2017**, *114*, 74–81. [CrossRef]

26. Li, H.; Liu, M.; Liu, Q. The effect of non-polar oil on fine hematite flocculation and flotation using sodium oleate or hydroxamic acids as a collector. *Miner. Eng.* **2018**, *119*, 105–115. [CrossRef]

27. Yoon, R.-H.; Flinn, D.H.; Rabinovich, Y.I. Hydrophobic interactions between dissimilar surfaces. *J. Colloid Interface Sci.* **1997**, *185*, 363–370. [CrossRef]

28. Israelachvili, J.; Pashley, R. The hydrophobic interaction is long range, decaying exponentially with distance. *Nature* **1982**, *300*, 341–342. [CrossRef] [PubMed]

29. Hu, Y.; Qiu, G.; Miller, J. Hydrodynamic interactions between particles in aggregation and flotation. *Int. J. Miner. Process.* **2003**, *70*, 157–170. [CrossRef]

30. Hoek, E.M.; Agarwal, G.K. Extended DLVO interactions between spherical particles and rough surfaces. *J. Colloid Interface Sci.* **2006**, *298*, 50–58. [CrossRef]

31. Li, Y.; Zhu, H.; Li, W.; Zhu, Y. A fundamental study of chalcopyrite flotation in sea water using sodium silicate. *Miner. Eng.* **2019**, *139*, 105862. [CrossRef]

32. Derjaguin, B.; Landau, L. Theory of the stability of strongly charged lyophobic sols and of the adhesion of strongly charged particles in solutions of electrolytes. *Prog. Surf. Sci.* **1993**, *43*, 30–59. [CrossRef]

33. Tong, K.; Song, X.; Xiao, G.; Yu, J. Colloidal processing of $Mg(OH)_2$ aqueous suspensions using sodium polyacrylate as dispersant. *Ind. Eng. Chem. Res.* **2014**, *53*, 4755–4762. [CrossRef]

34. Oss, C.J.V.; Giese, R.F.; Costanzo, P.M. DLVO and non-DLVO interactions in hectorite. *Clays Clay Miner.* **1990**, *38*, 151–159. [CrossRef]

35. Feng, B.; Lu, Y.; Feng, Q.; Li, H. Solution chemistry of sodium silicate and implications for pyrite flotation. *Ind. Eng. Chem. Res.* **2012**, *51*, 12089–12094. [CrossRef]

36. Wang, Y.; Chen, X.; Hu, Y.; Lan, Y. Influences of phosphates on dispersion of fine alumin-silicate minerals. *J. Cent. South Univ. (Sci. Technol.)* **2007**, *38*, 238–244.

37. Xu, D.; Zhu, S.; Cao, G.; Cui, H. Influences of sodium hexametaphosphate on dispersion of fine montmorillonite in coal flotation. *J. China Coal Soc.* **2016**, *41*, 192–198. [CrossRef]

38. Mao, L. *Application of Extended DLVO Theory: Modeling of Flotation and Hydrophobicity of Dodecane*; Virginia Polytechnic Institute and State University, Virginia Tech: Blacksburg, VA, USA, 1998.

39. Perdew, J.P.; Wang, Y. Accurate and simple analytic representation of the electron-gas correlation energy. *Phys. Rev. B* **1992**, *45*, 13244–13249. [CrossRef]

40. Laasonen, K.; Pasquarello, A.; Car, R.; Lee, C.; Vanderbilt, D. Car-Parrinello molecular dynamics with Vanderbilt ultrasoft pseudopotentials. *Phys. Rev. B* **1993**, *47*, 10142–10153. [CrossRef]

41. Methfessel, M.; Paxton, A.T. High-precision sampling for Brillouin-zone integration in metals. *Phys. Rev. B* **1989**, *40*, 3616. [CrossRef]

42. Gerasimov, G.Y.; Losev, S.A. Kinetic models of combustion of kerosene and its components. *J. Eng. Phys. Thermophys.* **2005**, *78*, 1059–1070. [CrossRef]

43. Wei, Z.; Li, Y.; Xiao, Q.; Song, S. The influence of impurity monovalent cations adsorption on reconstructed chalcopyrite (001)-S surface in leaching process. *Minerals* **2016**, *6*, 89. [CrossRef]

44. Lucay, F.; Cisternas, L.A.; Gálvez, E.D.; López-Valdivieso, A. Study of the natural floatability of molybdenite fnes in saline solutions and effect of gypsum precipitatio. *Miner. Metall. Process.* **2015**, *32*, 203–208. [CrossRef]

45. Jacques, S.; Greet, C.; Bastin, D. Oxidative weathering of a copper sulphide ore and its influence on pulp chemistry and flotation. *Miner. Eng.* **2016**, *99*, 52–59. [CrossRef]

46. Muganda, S.; Zanin, M.; Grano, S. Influence of particle size and contact angle on the flotation of chalcopyrite in a laboratory batch flotation cell. *Int. J. Miner. Process.* **2011**, *98*, 150–162. [CrossRef]

47. Li, Y.; Lartey, C.; Song, S.; Li, Y.; Gerson, A.R. The fundamental roles of monovalent and divalent cations with sulfates on molybdenite flotation in the absence of flotation reagents. *RSC Adv.* **2018**, *8*, 23364–23371. [CrossRef]

48. Liao, Y.F.; Mao-Yan, A.N.; Xia, W.C. Reaserch on kerosene emulsifier as collector in fine coal flotation. *Clean Coal Technol.* **2010**, *16*, 17–19.

49. Rebolledo, E.; Laskowski, J.S.; Gutierrez, L.; Castro, S. Use of dispersants in flotation of molybdenite in seawater. *Miner. Eng.* **2017**, *100*, 71–74. [CrossRef]

50. Li, Y.; Yang, X.; Fu, J.; Li, W.; Hu, C. New insights into the beneficial roles of dispersants in reducing negative influence of Mg2+ on molybdenite flotation. *RSC Adv.* **2020**, *10*, 27401–27406. [CrossRef]

51. Lim, D.-H.; Wilcox, J. DFT-Based study on oxygen adsorption on defective graphene-supported Pt nanoparticles. *J. Phys. Chem. C* **2011**, *115*, 22742–22747. [CrossRef]